

PAPER

Global Alfvén eigenmode scaling and suppression: experiment and theory

To cite this article: E.D. Fredrickson *et al* 2018 *Nucl. Fusion* **58** 082022

View the [article online](#) for updates and enhancements.

Related content

- [Energetic particles in spherical tokamak plasmas](#)
K G McClements and E D Fredrickson
- [Observation of global Alfvén eigenmode avalanche events on the National Spherical Torus Experiment](#)
E.D. Fredrickson, N.N. Gorelenkov, E. Belova et al.
- [Observation of compressional Alfvén eigenmodes](#)
W.W. Heidbrink, E.D. Fredrickson, N.N. Gorelenkov et al.

Global Alfvén eigenmode scaling and suppression: experiment and theory

E.D. Fredrickson, E.V. Belova, N.N. Gorelenkov, M. Podestà¹, R.E. Bell, N.A. Crocker¹, A. Diallo, B.P. LeBlanc and the NSTX-U team

Princeton Plasma Physics Laboratory, Princeton, NJ 08543, United States of America

¹ Department of Physics and Astronomy, University of California, Los Angeles, CA 90095, United States of America

E-mail: efredrickson@pppl.gov

Received 4 December 2017, revised 26 April 2018

Accepted for publication 21 May 2018

Published 29 June 2018



Abstract

The spherical tokamak NSTX has been upgraded to include a second neutral beam line, with three independent beam sources, and to be capable of higher toroidal fields and longer duration plasmas (Ono *et al* 2015 *Nucl. Fusion* **55** 073007). In this paper we describe some of the initial observations of the effect that the higher field and the modified fast-ion distributions have had on the nature of the global Alfvén eigenmodes (GAE). We also report that the GAE excited through a Doppler-shifted ion cyclotron resonance (DCR) were suppressed in a large number of shots with the injection of a small amount of high pitch ($V_{||}/V$) fast ions, consistent with the predictions of an analytic theory (Gorelenkov *et al* 2003 *Nucl. Fusion* **43** 228). We show that the experimental scaling of the GAE frequency and toroidal mode numbers with toroidal field is qualitatively consistent with the predictions of the analytic theory, providing validation for the DCR model. The observed suppression of GAE has also been reproduced in simulations with the hybrid ideal stability code HYM (Belova *et al* 2017 *Phys. Plasmas* **24** 042505).

Keywords: GAE, Doppler-shifted ion-cyclotron resonance, NSTX-U

(Some figures may appear in colour only in the online journal)

1. Introduction

To maintain the plasma temperatures needed for thermonuclear fusion, reactors such as ITER [1] will need to confine a population of super-thermal fusion products for the time needed for them to transfer their energy to the thermal plasma. This non-thermal population of fast ions provides a large source of free energy available to drive instabilities. In fusion reactors relying on magnetic confinement of the plasma, the super-thermal ions are also expected to be super-Alfvénic, that is able to interact resonantly with a variety of Alfvénic instabilities. Alfvénic instabilities redistribute fast ions in energy, pitch-angle and in radial position, which in turn affects the current profile and how they heat the thermal plasma [2–5]. The instabilities can also potentially directly affect thermal energy transport [6, 7]. Thus there is considerable interest in developing the tools to predict the stability or

instability of Alfvénic fast-ion driven instabilities and model their potential effect on the fast ion population.

Beam heated spherical tokamaks (START [8], NSTX [9], MAST [10] and Globus-M [11]), which routinely operate with super-Alfvénic populations of beam ions [12], generally report a broader range of Alfvénic instabilities than are typically seen in conventional tokamaks [3]. In addition to the lower frequency Alfvénic modes previously studied in conventional aspect ratio tokamaks, e.g. toroidal and ellipticity-induced Alfvén eigenmodes (TAE/EAE) [13, 14], modes with frequencies extending up to the ion cyclotron frequency are seen. In figure 1 the most common of these higher frequency instabilities, the compressional and global Alfvén eigenmodes (CAE/GAE) [15–20] from a beam-heated NSTX plasma are shown. The recent observation that the GAE could be suppressed with the deposition of nearly tangential beam ions [21] has motivated numerical simulations and an extensive

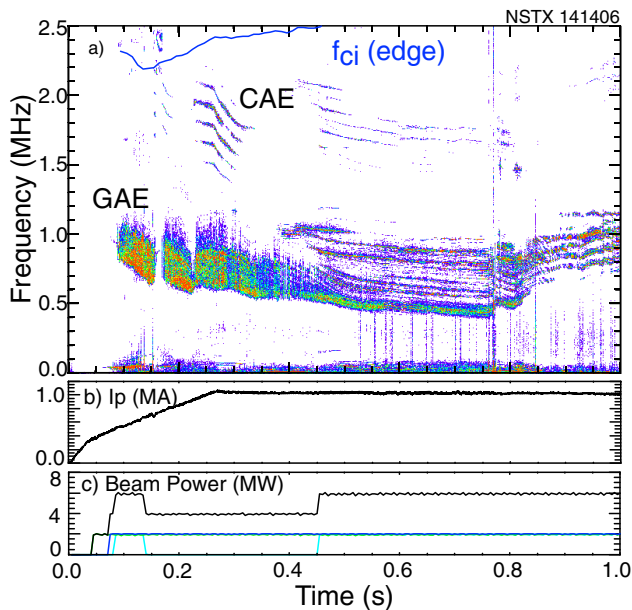


Figure 1. (a) spectrogram of magnetic sensor signal, (b) plasma current, (c) injected power from each of the three neutral beam sources.

comparison of the predictions of an analytical Doppler-shifted cyclotron resonance (DCR) stability model [7] with experimental observations.

In this paper we compare the frequency and toroidal mode number scaling of GAE to the predictions to help validate the analytic DCR model. We also report experimental observations of a novel technique used to suppress a specific Alfvénic instability on NSTX-U, the GAE excited through the DCR. These observations are interpreted in the context of the DCR model and with simulations using the unique hybrid magneto-hydrodynamic (MHD) code HYM [5, 22, 23].

The suppression experiments were made possible by the addition of a second neutral beam line (BL-2) which has three new neutral beam sources injected with tangency radii of $R_{\text{tan}} = 1.1$ m, 1.2 m and 1.3 m, that is with R_{tan} greater than the radius of the plasma magnetic axis, $R_{\text{axis}} \approx 1.05$ m. The original neutral beam sources have tangency radii smaller than the magnetic axis, $R_{\text{tan}} \approx 0.5$ m, 0.6 m and 0.7 m. The larger tangency radius of the new beam sources means that the beam ions are deposited on trajectories more parallel to the equilibrium magnetic field, thus with higher pitch (V_{\parallel}/V). In addition to the new sources, the first campaign on NSTX-U was run with a nominal toroidal field strength of ≈ 5.7 kG or 5.9 kG, up from the nominal maximum field on NSTX of ≈ 4.65 kG. The higher field increases the Alfvén velocity and lowers the ratio of the beam ion velocity to the Alfvén velocity.

2. Experimental results

While NSTX-U was run mostly with a nominal toroidal field strength of ≈ 5.9 kG, NSTX experiments covered a toroidal field range from 2.64 kG up to 4.65 kG (here, the toroidal field is defined as the vacuum field at a major radius of 1 m, close

to the typical radius of the magnetic axis). In experiments on NSTX, the GAE toroidal mode numbers, measured with an array of Mirnov coils [24], and frequency are both seen to scale positively with the toroidal field. This is seen anecdotally in figure 2 where spectrograms are shown for three NSTX plasmas with nominal toroidal fields of 2.65 kG, 3.8 kG and 4.65 kG. The spectrograms are color coded to indicate toroidal mode numbers. In these figures, the lowest frequency band of modes are chirping and are assumed to be GAE. The various modes at frequencies above this band include non-chirping modes and these modes are assumed to be a mix of GAE and CAE [25]. There may be multiple bands or modes with the same toroidal mode number, particularly evident in figures 2(a) and (b); presumably these represent the same toroidal mode number, but with a different poloidal structure.

The dominant GAE mode numbers increase from $n = 5$ and 6 at 2.65 kG, up to $n = 9$ and 10 at 4.65 kG. Likewise the GAE frequency increases from a range of 0.3–0.5 MHz up to 0.7 MHz to 0.8 MHz at 4.65 kG. To demonstrate this scaling, a database was constructed from NSTX H-mode shots heated by 90 kV neutral beams during the current flattop phase. At each Thomson scattering time, that is, approximately every 17 ms, the average toroidal mode number was calculated, weighted by the square of the mode amplitude. A similarly weighted average GAE frequency was calculated. The database contains more than 1200 time points from the multiple shots. The toroidal mode numbers versus toroidal field are shown in figure 3. Rather than plot the individual points, the n 's were averaged for all points, and the standard deviation was calculated, for each value of toroidal field and plasma current. The increase in average toroidal mode number is nearly linear with toroidal field. The last points (open circles) in figure 3 are from a similar analysis for NSTX-U H-mode shots. The black dashed line is a simple linear fit to the data. The blue point is from an NSTX-U L-mode plasma that will be discussed below.

The frequency of the dominant GAE also increases with toroidal field (figure 4). While it is not surprising to see a nearly linear scaling of the frequency of an Alfvén wave with toroidal field, it is interesting that the frequencies of the dominant *unstable* modes show this scaling. The dominant modes would, of course, be determined by resonant drive by the non-thermal fast-ion population.

3. GAE in NSTX-U

GAEs are also common in NSTX-U plasmas with the higher toroidal field, but not in plasmas heated with the new NSTX-U beam sources. The new sources are referred to here as beam line 2 (BL-2) sources. To illustrate this observation, a database was created from all NSTX-U shots in the last half of the 2016 experimental campaign, that is shot numbers between 204500 and 205088. Earlier shots were excluded as the power supplies used for the error-field compensation system introduce large amplitude, broad-band noise in the test cell. A noise compensation technique was introduced midway through the

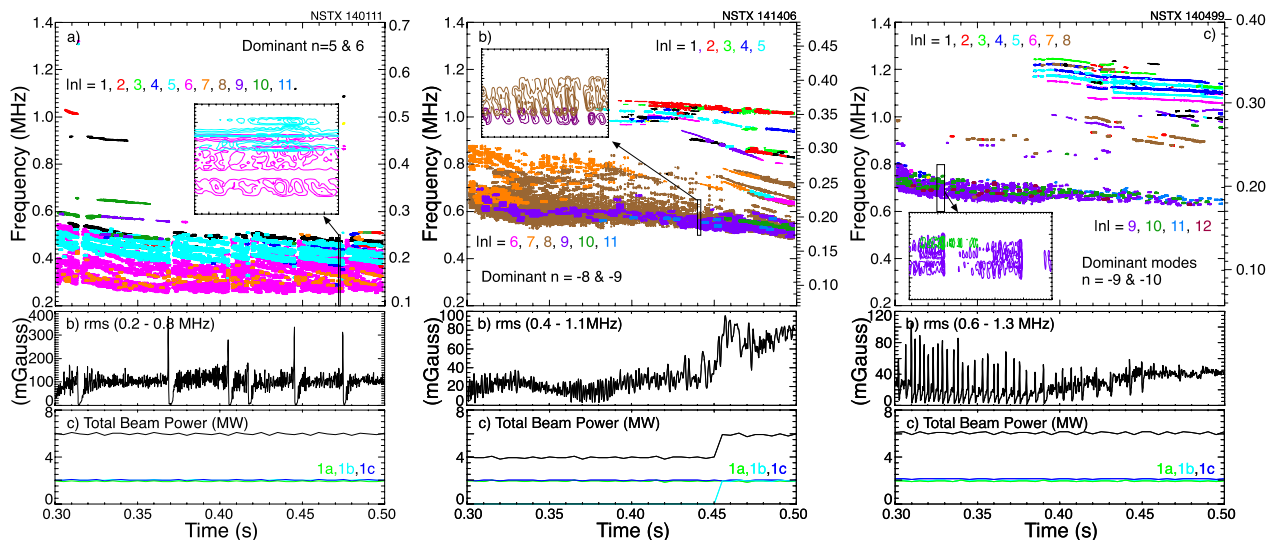


Figure 2. (a) spectrogram of magnetic fluctuations, rms fluctuation level and beam power from a 2.65 kG toroidal magnetic field plasma ($I_p = 0.71$ MA, $n_e = 5.15 \times 10^{13}/\text{cm}^3$). The colors in the spectrogram indicate toroidal mode number with the dominant modes being $n = -5$ (cyan) and $n = -6$ (magenta), (b) similar data for a 3.8 kG field shot ($I_p = 1.0$ MA, $n_e = 6.24 \times 10^{13}/\text{cm}^3$) where the dominant GAE have $n = -7$ (orange), $n = -8$ (brown) and $n = -9$ (purple), for a 4.65 kG field shot ($I_p = 1.1$ MA, $n_e = 5.8 \times 10^{13}/\text{cm}^3$) with dominant toroidal mode numbers of $n = -9$ (purple) and $n = -10$ (green). The scale on the r.h.s. of each spectrogram shows the frequency normalized to the ion cyclotron frequency on axis. (All beams at 90kV.) Insets in each figure expand the spectrograms for the regions in the boxes, illustrating the chirping of the modes.

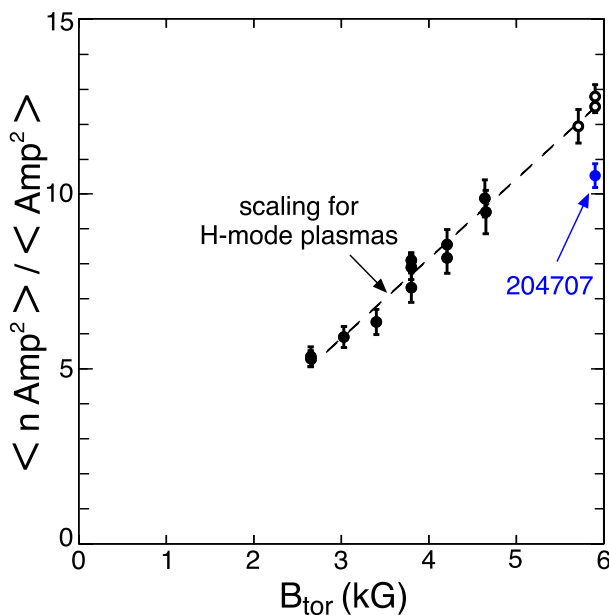


Figure 3. Scaling of the average toroidal number, weighted by the square of the amplitude, with toroidal field. Solid circles are from NSTX, open circles from NSTX-U. Blue point is from 0.4 s to 0.45 s of the NSTX-U L-mode shot discussed below.

campaign for shots after 204500. The database was created by computing the time averaged magnetic fluctuation spectrum around each Thomson scattering time.

For each Thomson scattering time point, the root-mean-square (rms) fluctuation level was calculated over the frequency range from 1 MHz up to 2.5 MHz. In NSTX-U, the GAE typically appear with frequencies near 2 MHz early in the discharge when the density is low and q_{min} is still high. The frequency drops towards 1 MHz as the density

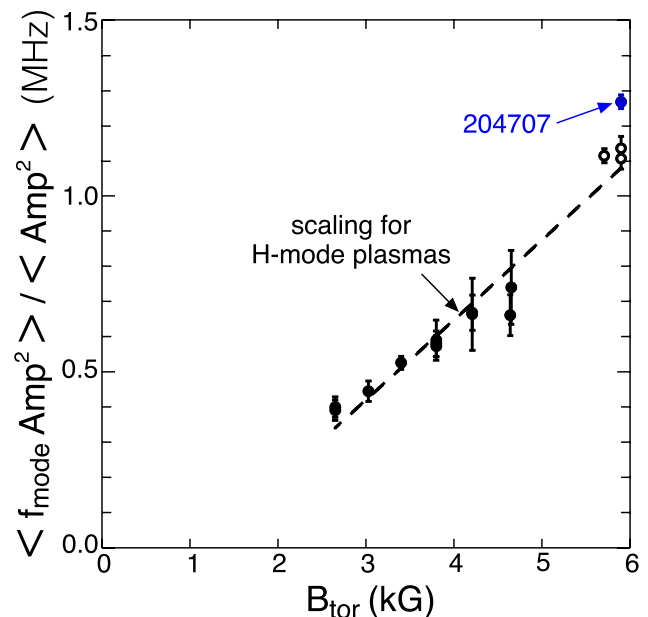


Figure 4. Scaling of the amplitude-weighted GAE frequency. Solid circles are NSTX, open circles are from NSTX-U shots. Blue point is from 0.4 s to 0.45 s of the NSTX-U L-mode shot discussed below.

rises and the plasma current evolves towards equilibrium, dropping q in the core. Calculating the rms fluctuation level over such a large frequency range adds a background level of 2 mG to 3 mG from plasma turbulence. In figure 5 the strong GAE, meaning those easily discriminated from quiescent plasmas, occur predominantly for plasmas where the total power from BL-2 is less than ≈ 0.15 MW. However, there are exceptions, meaning that the GAE are not strongly suppressed by BL-2 sources for all plasma conditions.

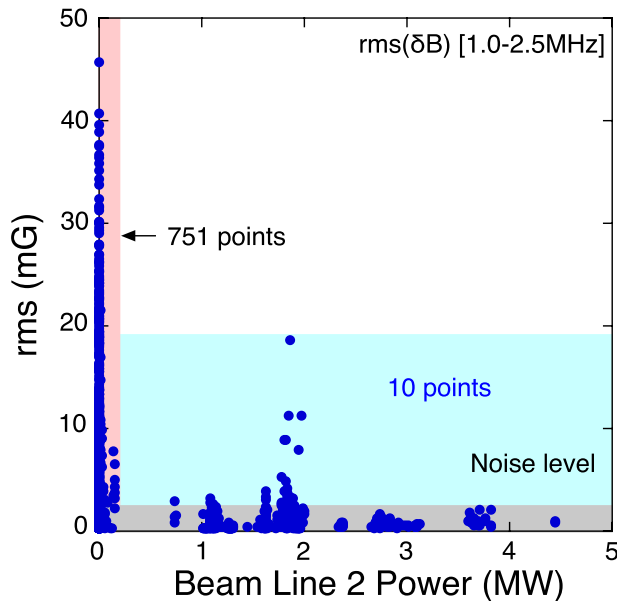


Figure 5. Root-mean-square magnetic fluctuation level in the GAE frequency range (1 MHz–2.5 MHz) versus beam power from the beam-line 2 sources.

Each of the three beam sources in BL-2 can be very effective at suppressing the GAE. In figure 6 is shown an example for each of the three BL-2 sources where power is added during existing GAE activity. In all three cases, the GAE are suppressed in <10 ms, and in figure 6(c) it can be seen that the GAE reappear shortly after BL-2 source 2c is turned off. The data presented here are not from controlled experiments, but from observations during other experiments. Thus, most examples of suppression occur early in the shot when beam sources are being added during the current ramp phase, as for these three examples shown in figure 6.

The potential effectiveness of BL-2 sources suppressing GAE is shown more clearly in figure 7 where a 20 ms window around the injection time of the BL-2 sources shows the rms amplitude of the GAE seen in figure 6. An effect on the GAE is seen within a few ms following the injection of a BL-2 source in figures 7(a) and (c). While the period between bursts increases soon after BL-2 injection in figure 7(b), the affect on the amplitude takes longer. As the slowing down time is greater than 50 ms, two things can be deduced from this figure. First, it takes relatively few high-pitch fast ions to suppress the GAE. Secondly, in these cases it can be assumed that the fast-ions responsible for the suppression have energies primarily near or just below, the full-energy or half-energy beam ions. As the high-pitch fast ions need to be resonant with the GAE to resonantly suppress the mode, examples with slower or less effective suppression may occur if the full or half energy ions are not resonant with the mode, but must slow down first. In which case, pitch-angle scattering may reduce the gradients responsible for mode suppression. The quick suppression of the GAE in these examples make a convincing case that the suppression is the result of changes in the fast-ion distribution.

We now consider examples where BL-2 sources are injected during existing GAE activity, that is ‘transition

events’. The transition events, as opposed to shot-to-shot comparisons with and without BL-2 sources, provide the cleanest data to develop an understanding of the suppression observations. Subtle shot-to-shot variations in machine and plasma conditions are avoided and the timescale for suppression is sufficiently short so that possible subtle equilibrium changes due to switching beam sources can be discounted. In the 2016 campaign there were over a hundred examples of either suppression of GAE with a BL-2 source injected into an existing GAE, or GAE appearing shortly after the cessation of BL-2 heating. In most cases injection of a BL-2 source into existing GAE activity resulted in complete suppression.

In figure 8 is shown a histogram of suppression at transition events where a BL-2 source was injected into an existing GAE. To more clearly show the magnitude of the drop, data where the pre-suppression GAE amplitude is less than 5 mG were excluded (the noise level is of order 2 mG). The drop is the difference between the rms amplitude averaged over 10 ms before BL-2 injection and the rms amplitude averaged from 20 ms to 30 ms after BL-2 injection to minimize the impact of cases where suppression is slower. The histogram shows the number of transition events corresponding to each range in fractional drop in amplitude. The events above 80% correspond to strong suppression of GAE. There are a significant number of events where the suppression is not complete (40%–80% drop in amplitude). Most of these events, the ones called out in red, occurred during a 2 d period in the campaign. Only a somewhat higher than normal oxygen level has so far been identified as a unique characteristic of these plasmas. Identifying the significant difference of this set of shots may help to clarify the optimum approach to suppression.

4. Analytic model of GAE suppression and drive

The observations reported above are qualitatively consistent with an analytic model of the DCR drive for GAE [7, 21]. The example of suppression of GAE shown in figures 6(c) and 7(c) is chosen to illustrate the application of this analytic theory. In figure 6(c) the GAE are suppressed shortly after source BL-2c is turned on at ≈ 0.206 s. The classic fast ion distribution functions before and after suppression were generated in TRANSP with NUBEAM [26]. The theoretical model of the DCR is evaluated 0.20 s and 0.21 s across the transition from unstable to stable. There is large uncertainty in the q profile, which is not measured in the NSTX-U shots, particularly during and shortly after the current ramp before the current has had time to equilibrate. Thus, figures 9 and 10 should be considered as representative examples illustrating which fast-ions are resonant with the GAE.

The analytic DCR resonance model predicts that resonant fast-ions will drive the mode if $1.9 < k_{\infty}\rho_L < 3.9$, where ρ_L is the fast-ion Larmor radius. Resonant fast-ions will be stabilizing for $k_{\infty}\rho_L < 1.9$ and $k_{\infty}\rho_L > 3.9$. We evaluate this condition by first identifying the resonant fast ions. The resonance condition for fast-ions, including the next order fast-ion drifts, is $\omega_{\text{GAE}} + |k_{\parallel}| \pm s/qR|V_{b\parallel}| = \omega_{\text{ci}}$. The strongest drive comes from the two side-band resonances with $s = \pm 1$ [7, 21],

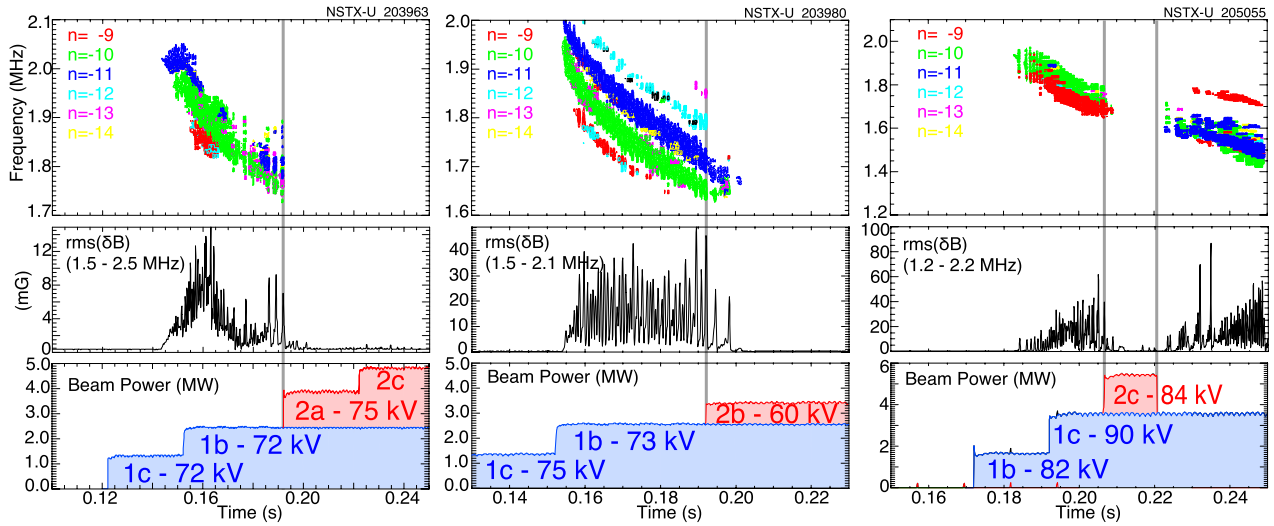


Figure 6. (a) Example of GAE being suppressed with the addition of beam source 2a (tangency radius 1.3m). (b) GAE suppressed with the addition of source 2b (tangency radius 1.2 m), and (c) GAE suppressed by the addition of source 2c (tangency radius 1.1 m), also shows that GAE can reappear when beam-line 2 power is turned off.

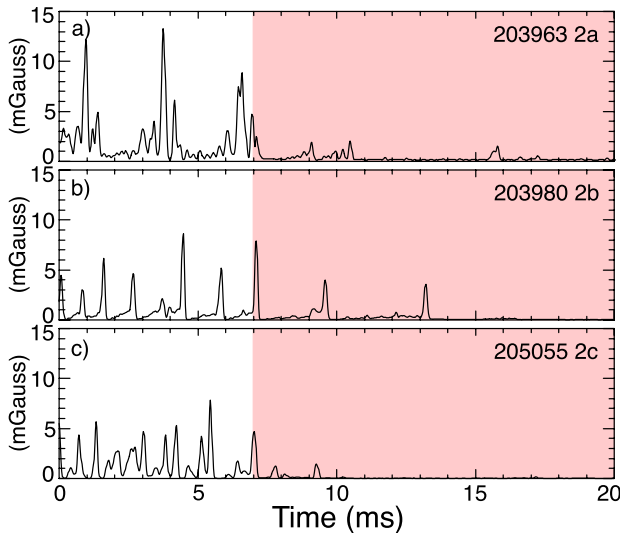


Figure 7. (a) rms amplitude of GAE for shot 203963, (b) rms GAE amplitude for shot 203980 and (c) rms GAE amplitude for shot 205055. The pink regions indicate when the outboard source is on. These are the three shots shown in figure 6.

although for NSTX plasmas often only the side-band corresponding to the slower parallel resonance velocity is important (see figure 10). This expression can be solved for $V_{b\parallel}$ if k_{\parallel} is known. We estimate k_{\parallel} from the dispersion relation for GAE, $\omega_{GAE} \approx \min\{\text{abs}[k_{\parallel}(r) V_{\text{Alfvén}}(r) + \ln\omega_{\text{rot}}(r)]\}$, where the minimum refers to the minimum in the dispersion relation radial profile. The Doppler correction to the measured mode frequency from the toroidal rotation of the plasma is included with the $\omega_{\text{rot}}(r)$ term. This is different than the Doppler shift in the resonance equation which comes from the parallel beam ion velocity.

We use the approximate cylindrical expression for k_{\parallel} , $k_{\parallel} \approx [m - n q(r)]/[R q(r)]$, and determine the m , or $k_{\perp} \approx m/r$, by fitting the dispersion relation to the measured mode frequency. This is illustrated in figure 9 where the profile of the dispersion relations for m 's from 6 to 10 are shown. The best

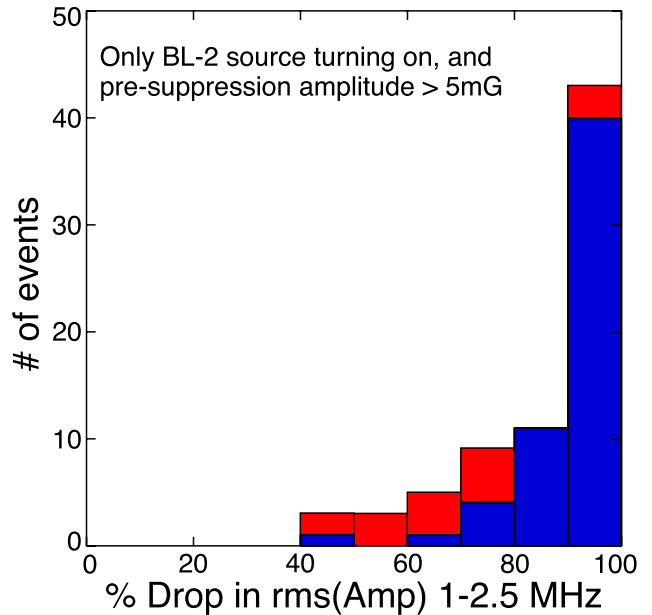


Figure 8. Histogram showing fractional drop in rms fluctuation level following application of one of the three beam-line 2 sources.

fit to the measured frequency is with $m = 8$. The presumed peak mode amplitude should be near the radial minimum in dispersion relation around $R = 117\text{cm}$ and the fast ion distribution functions shown in figure 10 are calculated for that region. The q -profile in this example is not measured, but comes from an equilibrium reconstruction, so this should be considered as illustrative as to how suppression occurs in this model.

The example of GAE suppression seen in figure 6(c) is used to illustrate which fast ions in the distribution function are resonant, and stabilizing or de-stabilizing. The distribution shown in figure 10(a) is typical for fast ions from beam-line 1. In contrast to the example shown in [21], figure 4, the suppression in this case occurs during the current ramp, with higher $q(0)$ and lower density. The suppression here appears

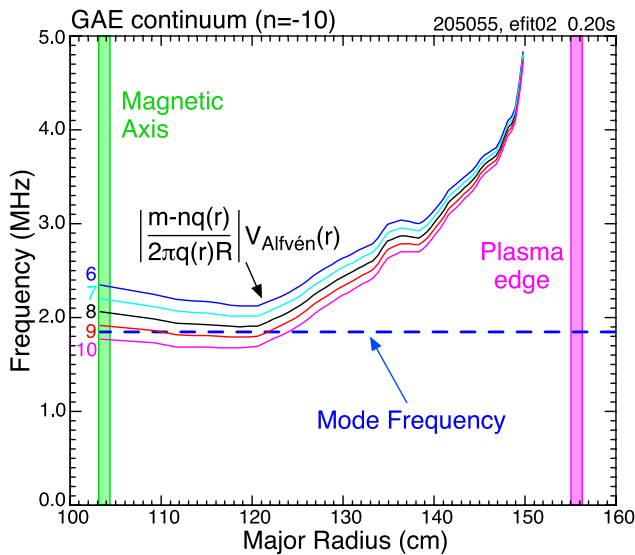


Figure 9. Profiles of the dispersion relation, including Doppler correction for plasma toroidal rotation, for the $n = -10$ GAE are shown for poloidal mode numbers $6 \leq ml \leq 10$ (colored curves as indicated). The observed mode frequency is indicated by the blue dashed line.

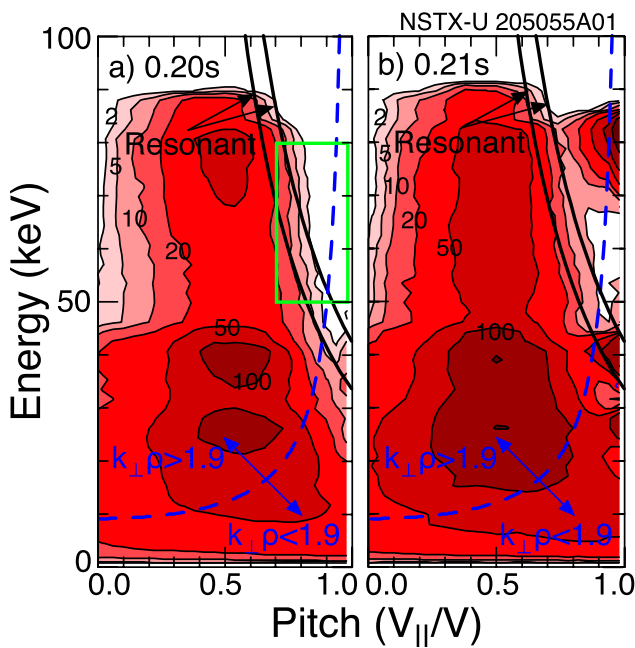


Figure 10. TRANSP fast-ion distributions before and after the outboard beam injection. The solid black lines indicate the two resonance solutions corresponding to $s = \pm 1$, the dashed blue line indicates fast ions with $k_{\infty}\rho_L = 1.9$. The distribution functions are calculated from $0.1 \leq r/a \leq 0.3$. Contours are labeled in units of $10^6/\text{cm}^3/\text{eV}/\text{dA}$. (a) Is the distribution at 0.2s, and (b) is the distribution at 0.21s.

to result from the high pitch, half-energy beam ion component, ≈ 42 keV, injected by source 2c. The delay in suppression sometimes seen may result from the need for the injected fast ions to slow down before becoming resonant. If a significant amount of slowing down is needed, e.g. 90 keV to 50 keV, pitch-angle scattering may make suppression less efficient.

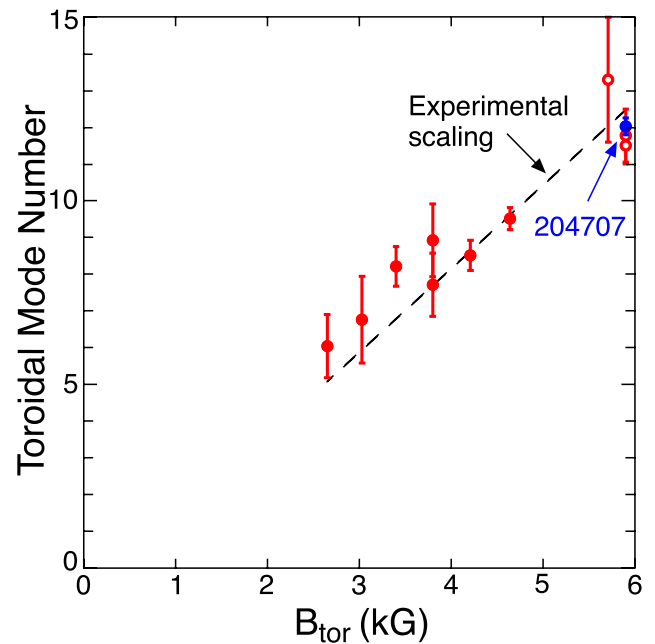


Figure 11. Predictions (red) of potentially unstable toroidal mode numbers, using the analytic model, for the shots in figure 4. Dashed line is experimental scaling for H-mode plasmas. Blue point is the simulation for 0.4 s to 0.45 s of the NSTX-U L-mode shot in figure 14.

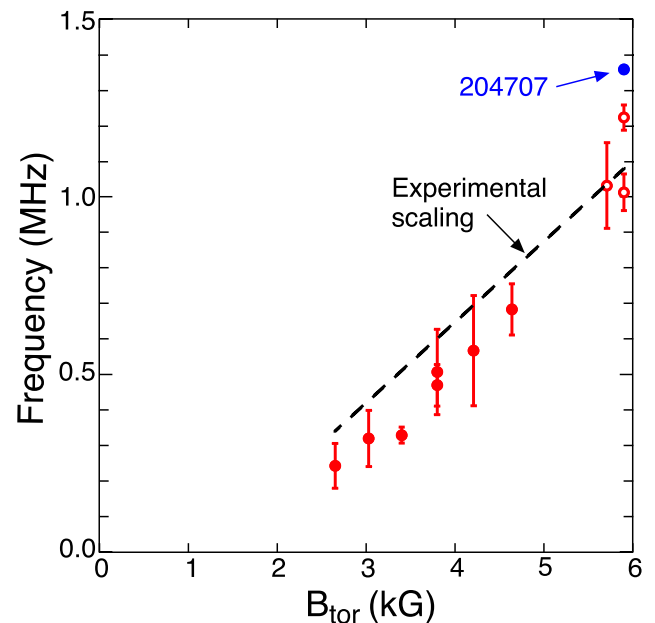


Figure 12. Predicted frequencies of unstable modes based on analytic theory (red points), black dashed line is the experimental scaling (figure 5). Blue point is for 0.4 s to 0.45 s of L-mode shot shown in figure 14.

A portion of the classical fast ion distribution functions calculated with NUBEAM in TRANSP at 0.20s and at 0.21s are shown in figure 10. The $V_{||}$ satisfying the resonance conditions for the $n = -10$ mode are indicated in figure 10 by the solid black curves with the lower curve corresponding to $s = +1$, and the upper curve for the $s = -1$ resonance. In this case both curves intersect a substantial fast ion population. Fast ions on the solid lines are resonant with the mode, but only those with

$1.9 \leq k_{\perp}\rho_L \leq 3.9$ will drive the GAE. The division is indicated by the blue dashed curve which shows where $k_{\perp}\rho_L \approx 1.9$, which is estimated using $m = 8$ and the minor radius of the minimum location. Fast ions along the black curves to the left of the blue-dashed line are destabilizing, to the right are stabilizing. As can be seen by comparing figures 10(a) and (b), the injection of BL-2c adds fast ions with pitch predominantly greater than 0.9, along the stabilizing part of the resonance curve. In this case it is interesting that it is the half-energy beam ions (≈ 45 keV) that are resonant with the $n = -10$ mode, and thus contribute towards stabilizing it. Neither the original distribution in figure 10(a), nor the distribution in figure 10(b) have had time to relax to a ‘slowing-down’ distribution, thus the ‘bump-on-tails’ at high pitch from BL-2c are still clearly visible.

The analytic theory can be tested by using it to predict the qualitative scalings of the GAE toroidal mode numbers and frequencies [7, 21] with toroidal field. The simple dispersion relation is used to predict mode frequencies, resonance curves and $k_{\perp}\rho_L = 1.9$ curves for a range of toroidal and poloidal mode number pairs (m, n). Modes that satisfy the constraint that the resonance (e.g. black curves in figure 10) and $k_{\perp}\rho_L = 1.9$ curves (e.g. blue dashed lines in figure 10) intersect in a reasonable range of fast ion energy and pitch are considered potentially unstable. The constraints used for figures 11 and 12 are that the resonance and the $k_{\perp}\rho_L = 1.9$ curves intersect in the phase-space region where $0.7 \leq V_{\parallel}/V \leq 0.97$ and $50 \text{ keV} \leq E_{\text{beam}} \leq 80 \text{ keV}$. These constraints are illustrated in figure 10(a) by the green rectangle.

With these constraints, the analytic theory has been applied to the representative NSTX shots shown in figure 3 during the current flattop phase and the NSTX-U shot shown in figure 13. The frequencies and mode numbers are averaged for all of the ‘unstable’ modes and shown in red in figures 11 and 12. The scaling shown in figures 3 and 4 are also included in figures 11 and 12. In agreement with the experiment, the range of toroidal mode numbers increases roughly linearly with toroidal field (figure 11). Similarly, the average frequencies of the ‘predicted’ unstable modes scale similar to the experimental scaling as shown in figure 12. The data here is from roughly similar H-mode shots in NSTX during the flattop period when the current profile had come to equilibrium and the density was relatively constant. The NSTX-U data is taken during the current flattop period of generally lower power H-modes. The blue point is from the period from 0.4 s to 0.45 s of the L-mode shot shown in figure 13. In both figures, the black dashed line is the linear fit to the experimental H-mode scaling data.

The suppression of the GAE at 0.45 s in figure 13 was modeled in [21]. Here we use the full GAE time evolution of the toroidal mode number and frequency, beginning when the suppressing beam source was turned off at 0.25 s and ending at 0.45 s when the suppressing source was turned back on. The time evolution of GAE frequency and mode numbers are predicted for this shot using the DCR model, which takes into account the evolution of the density increase and evolution of the q -profile.

In figure 13(a) is a spectrogram showing GAE activity for a 0.6 MA L-mode plasma on NSTX-U. Between 0.25 s and 0.45 s the density increases from $\approx 1.8 \times 10^{13}/\text{cm}^3$ to $\approx 3.5 \times$

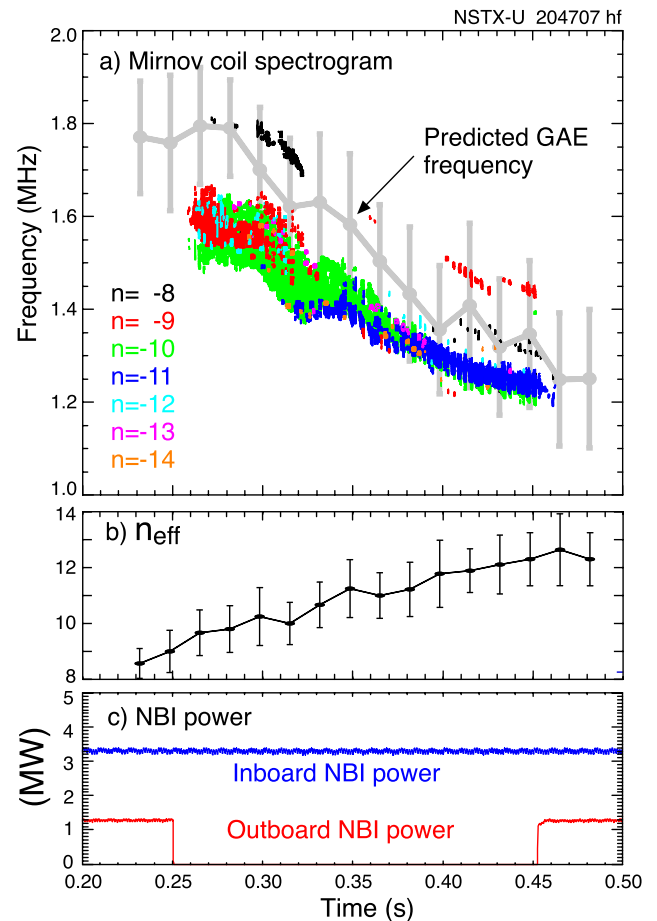


Figure 13. (a) Color-coded spectrogram showing counter-propagating GAE activity. Dominant modes evolve from $n = -9$ (red) and $n = -10$ (green) to $n = -10$ and $n = -11$ (blue), grey curve is predicted GAE frequency evolution (b) predicted GAE mode number evolution, (c) beam power, red curve is off-axis beam power (source 2c—72 kV), blue curve shows power from sources 1(a)—76 kV, 1(c)—87 kV.

$10^{13}/\text{cm}^3$ and $q(0)$ is calculated to drop from ≈ 1.8 to ≈ 1 . During that time the frequency decreases from ≈ 1.6 MHz at 0.2 s to ≈ 1.2 MHz at 0.45 s, roughly consistent with an Alfvénic scaling. The observed dominant mode numbers increase from $n = -9$ and $n = -10$ at 0.25 s to $n = -10$ and $n = -11$ at 0.45 s. Predictions with the DCR model over that time range are shown in figures 13(a) and (b). The algorithm used here implicitly assumes that there are no significant variations in the distribution function, and thus does not predict the GAE suppression before 0.25 s and after 0.45 s in figure 13. The predicted frequencies are uniformly somewhat high, but the overall evolution is roughly correct. The model over-predicts the increase in toroidal mode number with a prediction of an increase from $n_{\text{eff}} \approx 9$ at 0.25 s to $n_{\text{eff}} > 12$ at 0.45 s. This model is of course a local and quasi-cylindrical approximation and is not a stability analysis. Thus these results, while in good agreement with experimental measurements should be taken as only a qualitative prediction of the frequency and toroidal mode number scaling with toroidal field. The model qualitatively predicts the mode number and frequency trends of unstable GAE for NSTX and NSTX-U data, suggesting that the physics basis is reasonably accurate.

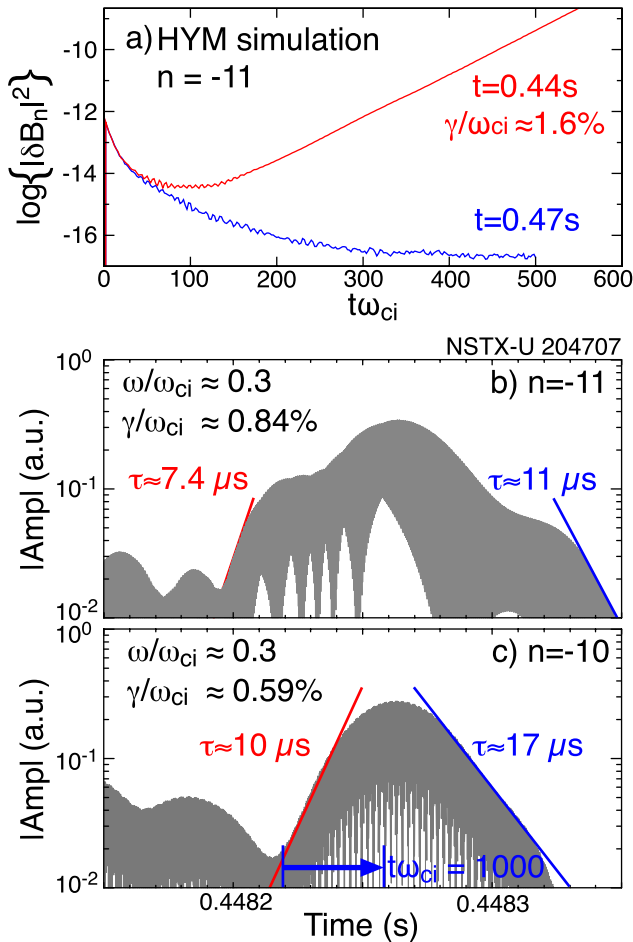


Figure 14. (a) Growth rates of $n = -11$ GAE as predicted with HYM at 0.44 s and 0.47 s, (b) experimental growth rate of $n = -11$ GAE burst and (c) of $n = -10$ GAE burst.

A more complete theoretical treatment of the GAE suppression is made with the hybrid ideal stability code, HYM, which reproduced the experimental stability observations. The HYM code [5, 22, 23] is unique in that it treats the beam ions using a full-orbit, delta- f particle model which allows HYM to capture the full ion-cyclotron resonance drive physics. HYM is a hybrid code in that it self-consistently couples the kinetic fast ion-model to a background plasma represented by one-fluid resistive MHD. HYM uses an analytic model for the fast-ion distribution with parameters chosen to fit TRANSP distribution functions [23]. Simulations with the HYM code matching TRANSP data at 0.44 s find the GAE with $n = -7$ through $n = -12$ unstable, in good agreement with experiment [21]. Matching the TRANSP data from 0.47 s, HYM finds the GAE stable, supporting the conclusion that changes to the fast-ion distribution are responsible for the GAE suppression.

The fast-ion distribution function used in HYM is an analytic approximation based on the TRANSP-NUBEAM calculation, which does not include, for example, the redistribution of fast-ions by the lower frequency TAE. Further, HYM does not include all potentially important damping terms for the GAE. We can compare the HYM calculations of the linear growth rates, figure 14(a), to experimental estimates of the drive and damping rates for the GAE made from the growth

and decay rates of the GAE bursts as shown in figures 14(b) and (c). The HYM calculation here uses a more accurate representation of the fast-ion distribution function from TRANSP which reduces the $n = -11$ growth rate from 2.3% as in [21], to 1.6%, in closer agreement with experimental estimates.

The growth rates from HYM simulations can be approximately compared to experimental growth rates, with the caveat that the HYM simulations do not include all known damping terms and the fast-ion distribution used in HYM is not experimentally measured. In figures 14(b) and (c) the magnetic fluctuations are digitally filtered to isolate the $n = -10$ and $n = -11$ GAE fluctuations. The absolute value of the fluctuations are plotted on a semi-logarithmic scale to more accurately determine the growth and damping rates than in [21]. The growth time, τ_{growth} , of the $n = -11$ burst is measured to be $\approx 7.4 \mu\text{s}$ and the decay rate, $|\tau_{\text{decay}}|$, is $\approx 11 \mu\text{s}$. With the assumption that the damping rate is constant, and that the growth rate of the burst is $\gamma_{\text{growth}} \approx \gamma_{\text{drive}} - |\gamma_{\text{damp}}|$, and that $|\gamma_{\text{damp}}| \geq |\gamma_{\text{decay}}|$, then $\gamma_{\text{drive}} \geq \gamma_{\text{growth}} + |\gamma_{\text{decay}}|$. For comparison to the simulation results, those numbers are normalized to the ion cyclotron frequency of $\approx 2.7 \times 10^7$ radians/s to get $\gamma_{\text{growth}}/\omega_{\text{ci}} \approx 0.6\%$ and $\gamma_{\text{drive}}/\omega_{\text{ci}} \approx 0.84\%$. A similar calculation for the $n = -10$ burst gives $\gamma_{\text{drive}}/\omega_{\text{ci}} \approx 0.59\%$ (compared to 0.5% quoted in [21]).

The GAE in figure 13 are avalanching [24], thus the bursts of the $n = -10$ and $n = -11$ modes are coupled, and in figure 14 it appears that the growth of the $n = -10$ mode is affecting the growth rate of the $n = -11$, so the comparison of theoretical and experimental growth rates should be considered qualitative at best. The onset of the $n = -10$ growth results in a plateau in the growth of the $n = -11$, which then resumes following the saturation of the $n = -10$. HYM is used here to model the linear growth of individual modes, whereas avalanches involve the non-linear interactions of multiple modes. Figure 14(c) is the same $n = -10$ burst used in figure 5(c), [21], but included here to provide evidence of nonlinear coupling of the $n = -10$ and $n = -11$ GAE during avalanching [24]. With these caveats, the experimental estimates of linear growth rates are in reasonable agreement with the HYM simulations given the uncertainties in the distribution function, the non-linear coupling of the GAE modes which could affect the growth rate and the need to include additional damping terms in the HYM simulations.

5. Summary

Counter-propagating GAEs, excited through a Doppler-shifted ion cyclotron resonance, were studied in the first experimental campaign on NSTX-U. The NSTX-U device is a major upgrade to NSTX, with higher toroidal field and a second neutral beam line, with three independent beam sources. The new sources inject higher pitch-angle fast ions, allowing much greater flexibility in generating the fast ion distribution. The higher pitch fast ions were found to very effectively suppress the GAE. The GAE also had higher frequencies and higher toroidal mode numbers than the GAE on NSTX. We have shown that the suppression of the GAE with higher pitch fast ions is consistent with an analytic theory describing the Doppler-shifted

cyclotron resonance drive for GAE [7]. The analytic theory was also used to predict a scaling of the frequency and the toroidal mode numbers with toroidal fields that is in good agreement with the experimental measurements. We have presented the results of simulations with a hybrid ideal stability code, HYM. The simulations both predicted the instability of the observed GAE before suppression, and the stabilization of those modes that were observed with the injection of the high pitch fast ions. These experimental validations of the analytic and numerical (HYM) models provide confidence in the predictions of fast-ion driven instabilities in future devices such as ITER.

Acknowledgment

Work supported by U.S. DOE Contract DE-AC02-09CH11466 and DESC-SC0011810.

Notice

This manuscript is based upon work supported by the U.S. Department of Energy, Office of Science, Office of Fusion Energy Sciences, and has been authored by Princeton University under Contract Number DE-AC02-09CH11466 with the U.S. Department of Energy. The publisher, by accepting the article for publication acknowledges, that the United States Government retains a non-exclusive, paid-up, irrevocable, world-wide license to publish or reproduce the published form of this manuscript, or allow others to do so, for United States Government purposes.

ORCID iDs

M. Podestà  <https://orcid.org/0000-0003-4975-0585>
 N.A. Crocker  <https://orcid.org/0000-0003-2379-5814>

References

- [1] ITER Physics Expert Group on Energetic Particles, Heating, and Current Drive and ITER Physics Basis Editors 1999 *Nucl. Fusion* **39** 2471
- [2] Gorelenkov N.N., Pinches S.D. and Toi K. 2014 *Nucl. Fusion* **54** 125001
- [3] McClements K.G. and Fredrickson E.D. 2017 *Plasma Phys. Control. Fusion* **59** 053001
- [4] Fisch N.J. and Rax J.-M. 1992 *Phys. Rev. Lett.* **69** 612
- [5] Belova E.V., Gorelenkov N.N., Fredrickson E.D., Tritz K. and Crocker N.A. 2015 *Phys. Rev. Lett.* **115** 015001
- [6] Stutman D., Delgado-Aparicio L., Gorelenkov N., Finkenthal M., Fredrickson E., Kaye S., Mazzucato E. and Tritz K. 2009 *Phys. Rev. Lett.* **102** 115002
- [7] Gorelenkov N.N., Fredrickson E., Belova E., Cheng C.Z., Gates D., Kaye S. and White R. 2003 *Nucl. Fusion* **43** 228
- [8] McClements K.G., Gryaznevich M.P., Sharapov S.E., Akers R.J., Appel L.C., Counsel G.F., Roach C.M. and Majeski R. 1999 *Plasma Phys. Control. Fusion* **41** 661
- [9] Fredrickson E.D. et al 2006 *Phys. Plasmas* **13** 056109
- [10] Gryaznevich M.P. et al (The MAST Team) 2008 *Nucl. Fusion* **48** 084003
- [11] Bakharev N.N. et al 2015 *Nucl. Fusion* **55** 043023
- [12] Fredrickson E.D., Gorelenkov N.N., Podesta M., Bortolon A., Gerhardt S.P., Bell R.E., Diallo A. and LeBlanc B. 2014 *Nucl. Fusion* **54** 093007
- [13] Cheng C.Z. and Chance M.S. 1986 *Phys. Fluids* **29** 2471
- [14] Zheng L.J. and Chen L. 1998 *Phys. Plasmas* **5** 444
- [15] Gorelenkov N.N., Cheng C.Z., Fredrickson E., Belova E., Gates D., Kaye S., Kramer G.J., Nazikian R. and White R. 2002 *Nucl. Fusion* **42** 977
- [16] Appert K., Gruber R., Troyon F. and Vaclavik J. 1982 *Plasma Phys.* **24** 1147
- [17] Mahajan S.M., Ross D.W. and Chen G.-L. 1983 *Phys. Fluids* **26** 2195
- [18] Van dam J.W., Fu G.Y. and Cheng C.Z. 1990 *Fusion Technol.* **18** 461
- [19] Belikov V.S., Kolesnichenko Y.I. and White R.B. 2003 *Phys. Plasmas* **10** 4771
- [20] Kolesnichenko Y.I., White R.B. and Yakovenko Y.V. 2006 *Phys. Plasmas* **13** 122503
- [21] Fredrickson E.D. et al 2017 *Phys. Rev. Lett.* **118** 265001
- [22] Belova E.V., Gorelenkov N.N. and Cheng C.Z. 2003 *Phys. Plasmas* **10** 3240
- [23] Belova E.V., Gorelenkov N.N., Crocker N.A., Lestz J.B., Fredrickson E.D., Tang S. and Tritz K. 2017 *Phys. Plasmas* **24** 042505
- [24] Fredrickson E.D. et al 2012 *Nucl. Fusion* **52** 043001
- [25] Crocker N.A. et al 2013 *Nucl. Fusion* **53** 043017
- [26] Pankin A., McCune D., Andre R., Bateman G. and Kritz A. 2004 *Comput. Phys. Commun.* **159** 157–84